Molecular Genetics and Metabolism 133 (2021) 201–210

Contents lists available at ScienceDirect

Molecular Genetics and Metabolism

journal homepage: www.elsevier.com/locate/ymgme

Characterization of a complex phenotype (fever-dependent recurrent acute liver failure and osteogenesis imperfecta) due to *NBAS* and *P4HB* variants

Francisco Javier Cotrina-Vinagre [a,1], María Elena Rodríguez-García [a,b,1], Elena Martín-Hernández [a,b,c], Cristina Durán-Aparicio [d], Abraham Merino-López [a], Enrique Medina-Benítez [d], Francisco Martínez-Azorín [a,b,*]

[a] Grupo de Enfermedades Raras, Mitocondriales y Neuromusculares (ERMN), Instituto de Investigación Hospital 12 de Octubre (i+12), E-28041 Madrid, Spain
[b] Centro de Investigación Biomédica en Red de Enfermedades Raras (CIBERER), U723, E-28041 Madrid, Spain
[c] Unidad Pediátrica de Enfermedades Raras, Enfermedades Mitocondriales y Metabólicas Hereditarias, Hospital 12 de Octubre, E-28041, Madrid, Spain
[d] Departamento de Pediatría, Unidad de Gastroenterología y Hepatología Pediátricas, Hospital 12 de Octubre, E-28041, Madrid, Spain

ARTICLE INFO

Article history:
Received 6 October 2020
Received in revised form 21 February 2021
Accepted 22 February 2021
Available online 27 February 2021

Keywords:
WES
NBAS
P4HB
Infantile liver failure syndrome 2 (ILFS2)
Cole-Carpenter syndrome 1 (CLCRP1)
COL1A2

ABSTRACT

We report the clinical, biochemical and genetic findings from a Spanish boy of Caucasian origin who presented with fever-dependent RALF (recurrent acute liver failure) and osteogenesis imperfecta (OI). Whole-exome sequencing (WES) uncovered two compound heterozygous variants in *NBAS* (c.[1265 T > C];[1549C > T]:p.[(Leu422Pro)];[(Arg517Cys)]), and a heterozygous variant in *P4HB* (c.[194A > G];[194=]:p.[(Lys65Arg)];[(Lys65=)]) that was transmitted from the clinically unaffected mother who was mosaic carrier of the variant. Variants in NBAS protein have been associated with ILFS2 (infantile liver failure syndrome-2), SOPH syndrome (short stature, optic nerve atrophy, and Pelger-Huët anomaly syndrome), and multisystem diseases. Several patients showed clinical manifestations affecting the skeletal system, such as osteoporosis, pathologic fractures and OI. Experiments in the patient's fibroblasts demonstrated that mutated NBAS protein is overexpressed and thermally unstable, and reduces the expression of *MGP*, a regulator of bone homeostasis. Variant in PDI (protein encoded by *P4HB*) has been associated with CLCRP1 (Cole-Carpenter syndrome-1), a type of severe OI. An increase of COL1A2 protein retention was observed in the patient's fibroblasts. In order to study if the variant in *P4HB* was involved in the alteration in collagen trafficking, overexpression experiments of PDI were carried out. These experiments showed that overexpression of mutated PDI protein produces an increase in COL1A2 retention. In conclusion, these results corroborate that the variants in *NBAS* are responsible for the liver phenotype, and demonstrate that the variant in *P4HB* is involved in the bone phenotype, probably in synergy with *NBAS* variants.

1. Introduction

NBAS (NBAS Subunit Of NRZ Tethering Complex) is a highly conserved gene that encodes NBAS (Neuroblastoma-amplified sequence) protein. This protein functions as a component of an endoplasmic reticulum (ER) tethering complex in the retrograde vesicular transport [1,2], as a mediator of the ER-NMD (nonsense-mediated mRNA decay) [3,4], and in the formation of large transport vesicle at the ER exit site in the secretory pathway [5]. A homozygous *NBAS* variant was described in an isolated population of Asia, which showed SOPH syndrome (short stature, optic nerve atrophy, and Pelger-Huët anomaly syndrome; MIM: 614800) [6]. Later, in 2015 the identification of homozygous or compound heterozygous variants in *NBAS* was reported in patients with fever-dependent RALF (recurrent acute liver failure) starting in infancy or ILFS2 (infantile liver failure syndrome-2; MIM: 616483) [2]. The disease is characterized by episodic liver failure precipitated by intercurrent febrile illness with liver function recovered completely between episodes. To date, a total of 126 patients from 112 families with 101 different variants in *NBAS* have been reported with a considerable phenotypic variability, from SOPH syndrome to isolated ILFS2 or in association with multisystemic disease [7–10]. The manifestations of the skeletal system have high prevalence in these patients, including osteoporosis (reduced bone mineral density), pathologic fractures and osteogenesis imperfecta (OI) [7,9,11].

* Corresponding author at: Francisco Martínez-Azorín, Grupo de Enfermedades Raras, Mitocondriales y Neuromusculares (ERMN), Instituto de Investigación Hospital 12 de Octubre (i+12), Centro de Actividades Ambulatorias (CAA), 6ª Planta, Bloque E, Avda. Córdoba s/n, E-28041 Madrid, Spain.
E-mail address: fmartinez@h12o.es (F. Martínez-Azorín).
[1] Equal contribution.

https://doi.org/10.1016/j.ymgme.2021.02.007
1096-7192/

P4HB gene (Prolyl 4-hydroxylase subunit beta) encodes for PDI (Protein Disulfide Isomerase) a ubiquitous and multifunctional protein. PDI functions as a redox catalyst and as a chaperone by preventing protein aggregation in the ER or by retaining proteins within the ER where necessary [12,13]. Cole-Carpenter syndrome-1 (CLCRP1; MIM: 112240) is a rare OI-like disorder that was first reported in 1987 in two unrelated patients presenting bone fragility with multiple fractures and normal intelligence [14]. These patients were later diagnosed genetically as carriers of the same heterozygous missense variant in *P4HB* [15]. Currently, a total of 8 CLCRP1 patients from 7 families with 4 different variants in *P4HB* have been reported [15–20].

Herein, we describe a patient presenting fever-dependent RALF and OI, in whom we identified two compound variants in *NBAS*, and a heterozygous missense variant in *P4HB* by WES.

2. Material and methods

2.1. Whole-exome sequencing (WES)

WES was performed (BGI-Hong Kong Co., Ltd) on genomic DNA obtained from the patient blood. Nuclear variants and indels were prioritized according to the following criteria: a) recessive model of pathogenesis: (i) variants that were rare in healthy individuals (allele frequency below 0.01) or new; (ii) variants predicted to modify protein function; (iii) variants consistent with a recessive model of pathogenesis. b) Dominant model of pathogenesis: (i) variants that were very rare in healthy individuals (allele frequency below 10^{-5}) or new; (ii) variants predicted to modify protein function; (iii) variants consistent with a dominant model of pathogenesis. Additional indications to prioritize the candidate genes were obtained by using predictive software scoring the likelihood of pathogenicity.

2.2. Sanger sequencing

The variants detected by WES in the patient were independently verified by Sanger sequencing in genomic DNA from the patient and his parents. Briefly, genomic DNA was purified from lymphocytes using the QIAamp DNA Mini Kit (Qiagen) including the treatment with RNase A. When necessary, saliva, urine and hair were used for genomic DNA purification. The target sites and the flanking sequences were amplified by PCR with specific primers (primers and conditions available upon request), and the PCR products were purified with the NZYGelpure Kit (NZYTech). Variant screening was performed by bidirectional sequencing using the BigDye Terminator v3.1 Cycle Sequencing Kit (Applied Biosystems) on an ABI 3730 DNA Analyzer (Applied Biosystems).

2.3. Cell culture

Fibroblasts and AD293 cells were maintained in DMEM with high glucose (4.5 g/L (25 mM) D-glucose) and L-glutamine (DMEM) supplemented with 10% (*v*/v) fetal bovine serum (FBS), 100 U/ml penicillin, 100 μg/ml streptomycin and 50 μg/ml uridine.

Subcellular fractionation of transfected AD293 cells was carried out as follows: the cell monolayer was washed, trypsinized and resuspended on ice in SFB buffer (20 mM HEPES [pH 7.4], 10 mM KCl, 2 mM $MgCl_2$, 1 mM EDTA, 1 mM EGTA, 1 mM DTT and protease and phosphatase inhibitor cocktails) for 15 min. Cells were then ruptured using an automatic mini-grinder during 20 s. The resulting cell homogenate was incubated on ice during 20 min, centrifuged at 720 ×*g* 5 min, and the supernatant collected as the cytoplasmic fraction. The remaining pellet (nuclear material) was resuspended in SFB, homogenized with 15 strokes in a 25G syringe and centrifuged at 1200 ×*g* 7 min. The pellet was resuspended in RIPA buffer (50 mM Tris HCl [pH 7.4], 150 mM NaCl, 1% (*v*/v) NP-40, 0.5% (*w*/*v*) Sodium Deoxycholate, 1 mM EDTA, 0.1% (w/v) SDS) and sonicated 10 s on ice at a power setting of 2, resulting in the nuclear fraction.

2.4. Western blot

The fibroblasts from the patient and the control, or AD293 cells were lysed, the protein concentrations were determined, separated by a gradient 4–20% (w/v) SDS-PAGE, transferred to PVDF membrane and then probed with antibodies against the different proteins. A goat anti-mouse or anti-rabbit was used as a secondary antibody. The western blot signals were quantified by densitometry using NIH Image J version 1.49 software, and the intensities were normalized with that of β-actin.

2.5. Antibodies

Antibodies included anti-NBAS (E94748, Enogene), anti-PDI (E90692, Enogene; MA3-019, Invitrogen), anti-COL1A2 (ab208638, Abcam), anti-USE1 (MBS7051497, MyBiosource), anti-GRP78/BIP (11587-1-AP, ProteinTech), anti-Vinculin (V9264, Sigma-Aldrich), anti-Histone H3 (D1H2) (4499, Cell Signaling Technology), anti-β-actin (A5316, Sigma), Goat anti-Rabbit IgG (H + L) secondary antibody HRP conjugate (31,460, ThermoFisher Scientific), Goat anti-Mouse IgG (H + L) secondary antibody HRP conjugate (31,430, ThermoFisher Scientific; A-11008, Invitrogen), Goat anti-Mouse IgG2a-FITC (M5906, MitoSciences) and Goat anti-Rabbit IgG (H + L) (Alexa Fluor 568) (A-11042, Invitrogen).

2.6. RNA isolation, cDNA synthesis and qRT-PCR

Total RNA was extracted from cell cultures using NucleoZOL (Macherey-Nagel). The reverse transcription (RT) was performed by using the NZY First-Strand cDNA Synthesis Kit (NZYtech) and the qRT-PCR reactions were performed using a Fast SYBR Green Master Mix (Applied Biosystems). The relative amount of *NBAS, MPG* and *SMG* cDNA with respect to *GAPDH* cDNA in the samples was calculated using the comparative cycle threshold (ΔΔCt) method (primers and conditions available upon request).

2.7. Plasmid construction and generation of stable cell lines

The ORF (open reading frame) of *P4HB* was PCR amplified by using specific primers and cDNA from the patient. The wild type and mutated ORF of *P4HB* were amplified and cloned into episomal plasmid pREP4 (Thermo Fisher Scientific). AD293 cells were plated 24 h prior to transfection with the indicated plasmids using JetPEI (PolyPlus transfection, VWR) according to the manufacturer's instructions. After 48 h, the cells were transferred to medium containing 100 μg/ml hygromycin B for several weeks and single clones were then isolated and expanded to obtain the stable cell lines.

2.8. Immunocytochemistry

AD293 cells grown on 13 mm glass coverslips with poly-L-Lysine were incubated in the presence of 50 μg/mL ascorbic acid for 24 h, and fixed with 4% (*v*/v) paraformaldehyde in NaCl/Pi for 10 min. Cells were permeabilized in 0.2% (v/v) Triton X-100 in 1× Phosphate-Buffered Saline (PBS) for 10 min, washed three times for 5 min in 1× PBS, blocked for 30 min with 1% (*w*/*v*) BSA in 1× PBS-T (0.1% (v/v) Tween-20), and incubated with primary antibodies anti-COL1A2 (Abcam), or anti-PDI (Invitrogen), at 1:500 dilution in 1% (w/v) BSA in 1× PBS-T for 16 h at 4 °C. Cells were washed three times for 5 min in 1× PBS, and then incubated with secondary antibody Goat anti-Mouse IgG2a-FITC (MitoSciences) for PDI and Goat Anti-Rabbit IgG H&L (Alexa Fluor 568) (Invitrogen) for COL1A2, at 1:500 dilution in 1× PBS for 1 h at room temperature. Cells were treated with DAPI (Sigma) at 1:1000 dilution prior to mounting in ProLong mounting medium

(ThermoFisher Scientific). Images were acquired with a confocal laser-scanning microscope (LSM510 META ConfoCor 3, Zeiss) for constant gain and offset and processed with Zen 2009 software (Zeiss).

2.9. Statistical analysis

Data were analyzed using the independent samples *t*-test, and *P* values lower than 0.05 were considered statistically significant.

3. Results

3.1. Case report

The Ethic Committee of the Instituto de Investigación Hospital 12 de Octubre (i + 12) approved the study, and a written informed consent was obtained from the patient's parents.

The Spanish patient is a 13-year-old boy with a long history of recurrent hepatitis and an osteogenesis imperfecta (OI) phenotype (Fig. 1). He was a 37 weeks term baby with no relevant family history born by a caesarean section because of malposition and antenatal bilateral femur fracture. His features were characteristic, with low ear implantation, triangular face, high forehead and mild micrognathia. He was born with low weight (*i.e.*, 2240 g, p3) and height (*i.e.*, 45 cm, p9), and this delay was maintained as he grew, being always below the 3rd percentile in height. The clinical picture was clearly similar to an OI type III, although no variants were found in *COL1A1* (Collagen Type I Alpha 1 Chain) or *COL1A2* (Collagen Type I Alpha 2 Chain). He suffered several pathologic fractures throughout the years: left humeral fracture at 5 months of age; fracture of right femur at 15 months, 2 and 4 years; fracture of left femur at 4 and 5 years, and multiple costal fractures (*i.e.*, densitometries practiced between the ages of 2 and 9 showed low bone mineral density). In connection with these, he presented dentinogenesis imperfecta. In spite of being treated with intravenous bisphosphonates since he was 18 months old, osteopenia and an extreme bone fragility remained. He needed to wear vertebral corset and also needed surgery for vertebral stabilization due to severe kyphoscoliosis. Later on, at the age of 12 years old he underwent surgery in order to stabilize pseudarthrosis in both femurs. Due to his underlying disease, he has suffered a delay in his motor skills, and most of the time he needs a wheelchair. From 3 months of age he has suffered frequent respiratory infections with recurrent bronchospasm, requiring hospital admission and oxygen therapy. Because of his thoracic deformities, he has needed nocturnal continuous positive airway pressure from the age of 9. The patient did not suffer any visual difficulties and the ophthalmologic revision did not show optic nerve atrophy. No evidence of leucocyte anomalies was observed in blood smear examinations.

Regarding the liver disease, he suffered several episodes of acute liver failure, and all of them involved fever, mostly during respiratory infections. The first crisis was identified at 19 months of age and, by the age of 3, he had suffered 4 episodes of acute liver failure which required admission in a PICU (pediatric intensive care unit). In each of the episodes, after the onset of fever, the liver enzymes were raised over 500 times their normal value with severe hypoglycemia and coagulopathy leading to gastrointestinal bleeding twice. Following aggressive management of the fever and support treatment for the liver function, his symptoms and liver tests always normalized, with no findings of liver disease in between the episodes. These crises seemed to improve as the boy grew up, although episodes of high liver enzymes associated with fever remain (fever-dependent ELT -elevated liver transaminases-), but usually with no coagulopathy or PICU admission (without acute liver failure). He only had two other severe episodes, at the age of 5 and 8. None of the studies done during and between the crises has revealed any cause for the liver failure, including cultures, serologies, complete metabolic screenings, liver and muscle biopsies and vascular studies. Analysis did not show any humoral or cellular immunologic deficiencies. Toxic causes were also discarded; the imaging of the liver has always been normal, except for mild hepatomegaly and liver hyperechogenicity. The patient has never had hyperglycemia or diabetes.

Currently, the patient shows multiple deformities secondary to fractures, mostly in the lower limbs and a short and small thorax, and further orthopedic surgeries will be required in the future. ELT crises have decreased notably and, during the last year, he has only been

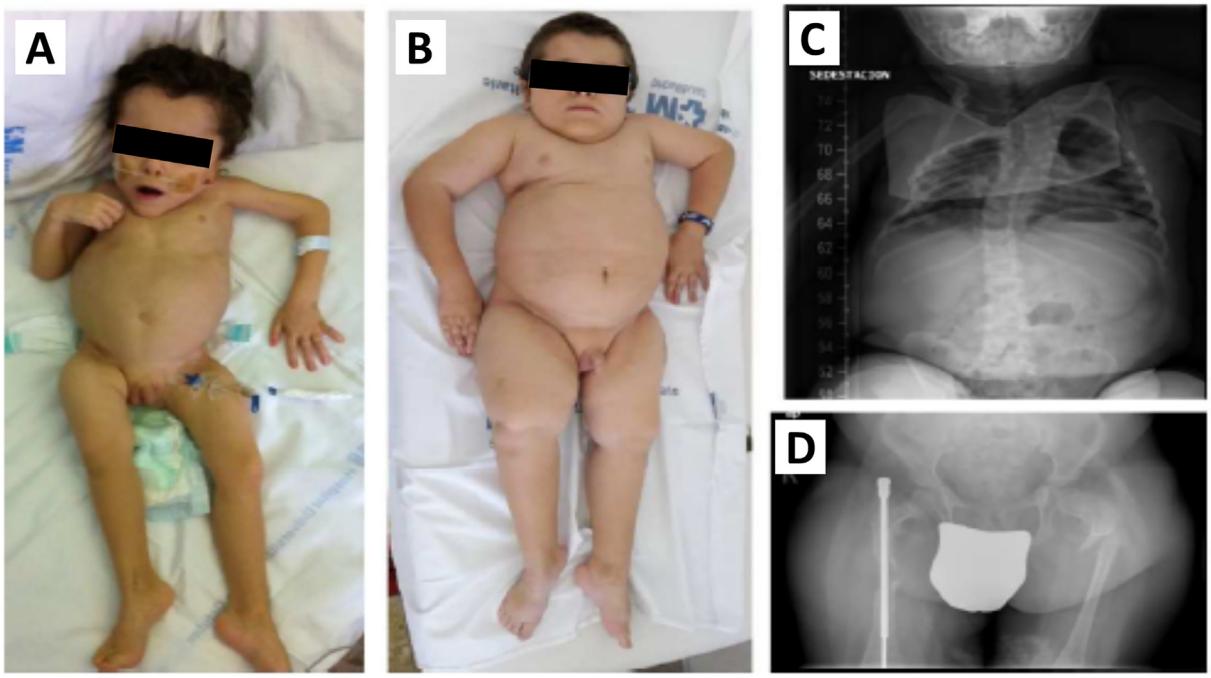

Fig. 1. Morphological characteristics of the patient. The patient at the age of 4 (A) and 8 years (B). He has severe short stature (−6.5 SD) and skeletal dysplasia with generalized osteopenia, scoliosis and thorax deformity and thin ribs, and has suffered numerous bone fractures since the neonatal age (C). He has hip dysplasia with dysplastic acetabulum and a broad femoral head with decentralization and pseudarthrosis (D). X rays were done at 6 years of age.

hospitalized once due to this issue. When not admitted, he has been attending both regular and a special needs school, developing acceptable language and social skills.

3.2. Exome sequencing

The analytic pipeline described in Material and Methods was used to prioritize WES variants in genes that were rare and were predicted to be deleterious (Table 1). We found two heterozygous missense variants with a recessive model of pathogenesis in *NBAS* (NM_015909.4: c.1265 T > C p.(Leu422Pro) and c.1549C > T p.(Arg517Cys)), and one heterozygous missense variant with a dominant model of pathogenesis in *P4HB* (NM_000918.4:c.194A > G p.(Lys65Arg)).

3.3. Characterization of NBAS variants

The compound heterozygous state of the variants c.1265 T > C and c.1549C > T in *NBAS* was assessed by Sanger sequencing. The patient carried bi-allelic variations in *NBAS*, whereas his healthy parents were heterozygous for only one allele of *NBAS* (Fig. 2A, B). The maternal c.1265 T > C (p.Leu422Pro) and the paternal c.1549C > T (p.Arg517Cys) variants were considered as "likely pathogenic" variant (Class 4) according to the ACMG guidelines. They are highly evolutionarily conserved from *Homo sapiens* to *Xenopus tropicalis* (Fig. 2C). The variant c.1265 T > C (p.Leu422Pro) is new and has not been reported in the gnomAD database, while the variant c.1549C > T (p.Arg517Cys) is listed with a low allele frequency of 1.6×10^{-5} (rs370526257) and without homozygous carriers. Both variants are located in the part of the protein that interacts with USE1 (Vesicle transport protein USE1), being one of them in the β-propeller domain and the other between the β-propeller and the secretory pathway Sec39 domains (Fig. 2D) [1].

3.4. Characterization of P4HB variant

The variant c.194A > G in *P4HB* was confirmed in heterozygous state by Sanger sequencing in the patient. In the father, the variant was absent, but in the mother, the variant was found to be in heterozygous state (Fig. 2E, F). A patient with CLCRP1 has previously been described with a variant in *P4HB* that was transmitted from his clinically unaffected father who was a mosaic carrier of the variant [15]. For this reason, genomic DNA extracted from other tissues different from blood (saliva, urine and hair) were sequenced. In hair, the relative area of the peak corresponding to the variant was lower in the mother (~38%G) than in the patient (~50%G) (Fig. 2F, hair). No differences were found in urine and saliva (~50%G) (data not shown). These results suggest that the mother is mosaic for this variant. The variant is listed in the gnomAD database with an extremely low allele frequency of 3.98×10^{-6} (rs753095561), but it has not been previously reported in any patient nor in homozygous carriers. The c.194A > G (p.Lys65Arg) was considered as "variant of uncertain significance (VUS)" (Class 3) according to the ACMG guidelines. The lysine 65 is also in a highly evolutionarily conserved from *Homo sapiens* to *Xenopus tropicalis* (Fig. 2G), and it is situated close to the active site of the Thioredoxin 1 domain of PDI protein (Fig. 2H).

3.5. Functional characterization of NBAS and PDI proteins

The effect of the variants in the expression of NBAS and PDI proteins was evaluated by western blot in skin fibroblasts by using a genetically unrelated control of similar age. The western blot was carried out first to detect NBAS (Fig. 3A, α-NBAS). The quantification of NBAS showed an increase of ~60% in the patient in comparison to the control (Fig. 3B). However, the steady-state levels of *NBAS* transcripts analyzed by qRT-PCR showed a ~ 25% decrease in the patient (Fig. 3C, *NBAS*). Later, the immunoblot was repeated to detect PDI, and the band of ~57 kDa appeared quantitatively normal in cells carrying the variant (Fig. 3A, α-PDI). Additional analysis of COL1A2 (Collagen alpha-2(I) chain) was performed since PDI is important for collagen type I processing, and reduced collagen secretion owing to *NBAS* variants could be responsible for the bone phenotype in the patient [9]. Two bands were detected, one of ~80 kDa that could be the mature COL1A2 (mCOL1A2, theoretical molecular weight 92 kDa), and other of ~160 kDa probably corresponding to the precursor (pCOL1A2; 129 kDa). Both bands were detected to a much higher extent in the patient than in the control (Fig. 3A, α-COL1A2).

The ER-NMD pathway requires the interaction of NBAS with the core NMD factor UPF1 (Regulator of nonsense transcripts 1) [4]. In order to study the effect of *NBAS* variants in the NMD pathway, the expression of *MGP* (Matrix Gla Protein) and *SMG5* (SMG5 Nonsense Mediated MRNA Decay Factor) genes was analyzed in the patient's cells (Fig. 3C, *MGP*, *SMG5*) [3]. The expression of both genes was significantly lower in the patient than in the control (Fig. 3C), suggesting that *NBAS* variants are affecting the NMD pathway in the patient. In addition, the downregulation of *MGP* would be compatible with the patient's bone phenotype (OI).

3.6. Thermal susceptibility of NBAS protein and ER stress

The ILFS2 in the patients with *NBAS* variants is characterized by recurrent episodes of acute liver failure precipitated by febrile illness. In order to investigate this point, fibroblasts from the patient and the control were subjected to a temperature shift from 37 to 40 °C during 24 or 48 h (Fig. 4). In the control fibroblasts, NBAS levels remained constant until 24 h at 40 °C, with a small, but not significant decrease at 48 h. However, the overexpression of NBAS at 37 °C of ~60% was eliminated after shifting to 40 °C. Thus, the levels of NBAS in the patient at 40 °C were significantly decreased to the levels of NBAS in the control (Fig. 4A, B). These results indicate a specific variant-dependent thermal instability of NBAS in the patient [21]. Since NBAS in humans is interacting with USE1 [1,2] the levels of this protein were also measured. Unlike NBAS, USE1 levels decreased at 37 °C in the patient, and this decrease was slightly greater at 40 °C (Fig. 4A, C).

Table 1
WES candidate gene Candidate variants after filtering and prioritization.

Chr	Position[a]	SNP	Ref	Status	Gene	Codon	Change	MAF[b]
Recessive model of pathogenesis								
2	15,614,241	rs370526257	G	Het[c]	***NBAS***[d]	CGC> TGC	Arg517Cys	1.6×10^{-5}
2	15,615,887	New	A	Het	***NBAS***	CTG> CCG	Leu422Pro	n.d.
Dominant model of pathogenesis								
17	79,817,215	rs753095561	T	Het	***P4HB***[e]	AAA> AGA	Lys65Arg	4.0×10^{-6}

[a] GRCh37.p13 (hg19).
[b] MAF: Minor Allele Frequency (from gnomAD browser).
[c] Het: Heterozygous; n.d.: no data.
[d] RefSeq NM_015909.4.
[e] RefSeq NM_000918.4.

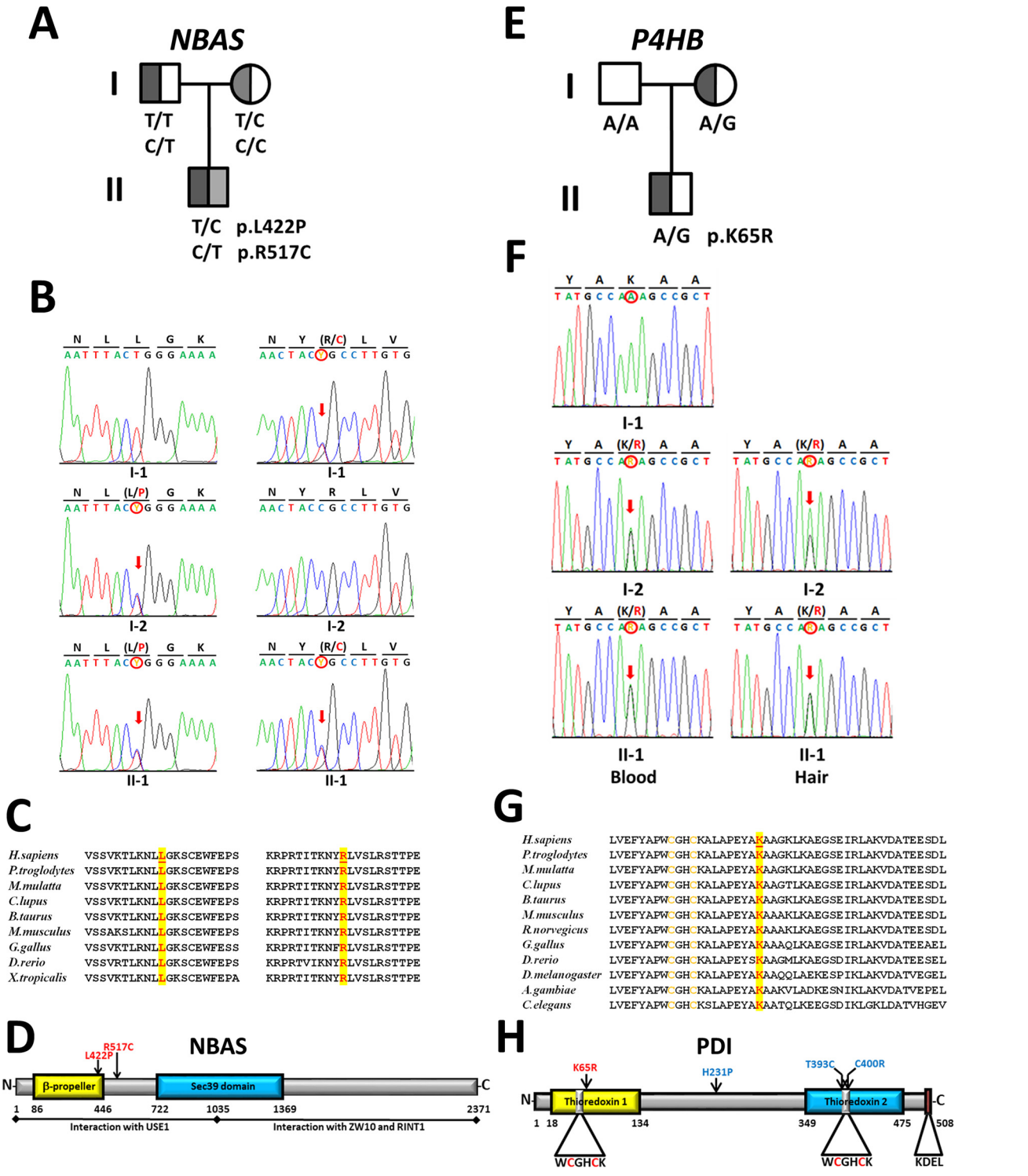

Fig. 2. Genetic analysis of *NBAS* and *P4HB*. (A) Family pedigree showing the genotype of the variants in *NBAS*. (B) Electropherograms showing Sanger sequencing validation of *NBAS* c.1265 T > C (p.L422P/p.Leu422Pro) and c.1549C > T (p.R517C/p.Arg517Cys) variants. (C) Multiple sequence alignment of NBAS region surrounding the p.L422P (red, left) and p.R517C (red, right) variants site in various species. (D) Schematic representation of NBAS showing the position of p.L422P and p.R517C variants (red, up). The structural features are shown: β-propeller and Sec39 domain (secretory pathway Sec39 domains), the USE1 interaction site at the N-terminus and the ZW10 and RINT1 interaction site at the C-terminus. (E) Family pedigree showing the genotype of the variant in *P4HB*. (F) Electropherograms showing Sanger sequencing validation of *P4HB* c.194A > G (p.K65R/p.Lys65Arg) variant in blood and in hair. (G) Multiple sequence alignment of PDI region surrounding the p.K65R (red) variant site in various species. (H) Schematic representation of PDI showing the position of p.K65R (red), p.H231P (p.His231Pro), p.T393C (p.Thr393Cys) and p.C400R (p.Cys400Arg) variants. The structural features are shown: Thioredoxin 1 and 2, and their active sites, and the endoplasmic reticulum (ER) retention motif (KDEL).

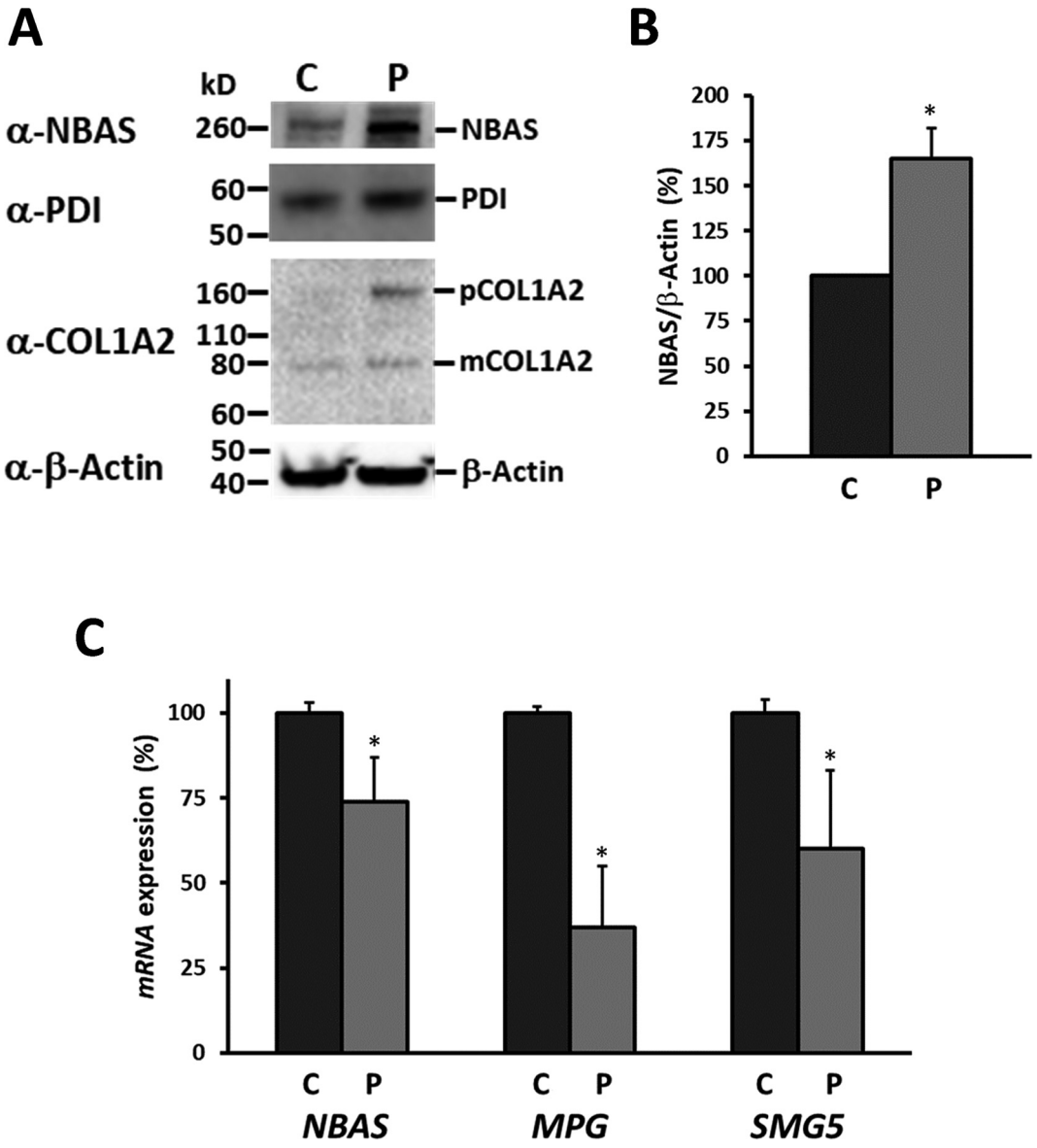

Fig. 3. Relative expression of proteins and genes in patient's fibroblasts. (A) Western blot analysis. Fibroblasts from the control (C) and the patient (P) were lysed, separated by SDS-PAGE, transferred to PVDF and probed with antibodies against NBAS, PDI, COL1A2 and β-actin. The panel shows a representative immunoblotting. pCOL1A2 is procollagen alpha-2(I), and mCOL1A2 is mature collagen alpha-2(I). (B) Quantification of NBAS protein levels normalized over β-actin. (C) qRT-PCR of *NBAS, MPG* and *SMG5* mRNA levels standardized against *GAPDH*. Data were the mean (±SD) of three independent experiments. $^{*}P < 0.05$.

In a previous report, the fibroblasts from NBAS deficient patients showed a significant increase in the expression of genes involved in ER stress response [2]. Following that finding, the expression of the ER stress marker protein GRP78 (Endoplasmic reticulum chaperone BiP) was quantified (Fig. 4A, D). Surprisingly, the expression of this protein, although slightly higher at 40 °C than at 37 °C, showed no significant changes between the control and patient cells, suggesting that ER stress is not induced by the NBAS variants.

3.7. Retention of COL1A2 into the cell is due to mutated PDI

The retention of COL1A2 in the cells could explain the OI in the patient. In order to investigate whether the retention of COL1A2 is due to the variant in *P4HB*, or the bone phenotype is due exclusively to the variants in *NBAS*, overexpression experiments of the wild-type and mutated version of PDI protein in AD293 cells were carried out (Fig. 5). Immunoblotting showed a higher expression of PDI when the AD293 cells were transfected with the plasmid containing the ORF of wild-type (*P4HB*-WT) or mutated PDI (*P4HB*-MUT) relative to the empty plasmid (Fig. 5A). Then, PDI expression and collagen retention (by staining of COL1A2) was studied by immunofluorescence (Fig. 5B). Quantification of the green fluorescence (Fig. 5B, PDI) showed again a higher expression in cells transfected with *P4HB*-WT or *P4HB*-MUT (Fig. 5C). However, COL1A2 retention was higher in cells overexpressing the mutated protein (Fig. 5B, COL1A2). Since the red fluorescence (COL1A2) was detected both in the cytoplasm and in the nucleus of *P4HB*-MUT cells and tenuously in nucleus of *P4HB*-WT cells, a subcellular fractionation into nuclear (Nu) and cytosolic (Cy) fractions was carried out, using Vinculin and Histone H3 as a cytoplasmic and nuclear markers respectively (Fig. 5D). The red fluorescence in the cytosolic fraction was due to mCOL1A2, while the signal in the nuclear fraction was due to COL1A2 C-terminal propeptide (C-propeptide; theoretical molecular weight ~ 28 kDa) [12]. The quantification of the red fluorescence in the cytosolic fraction

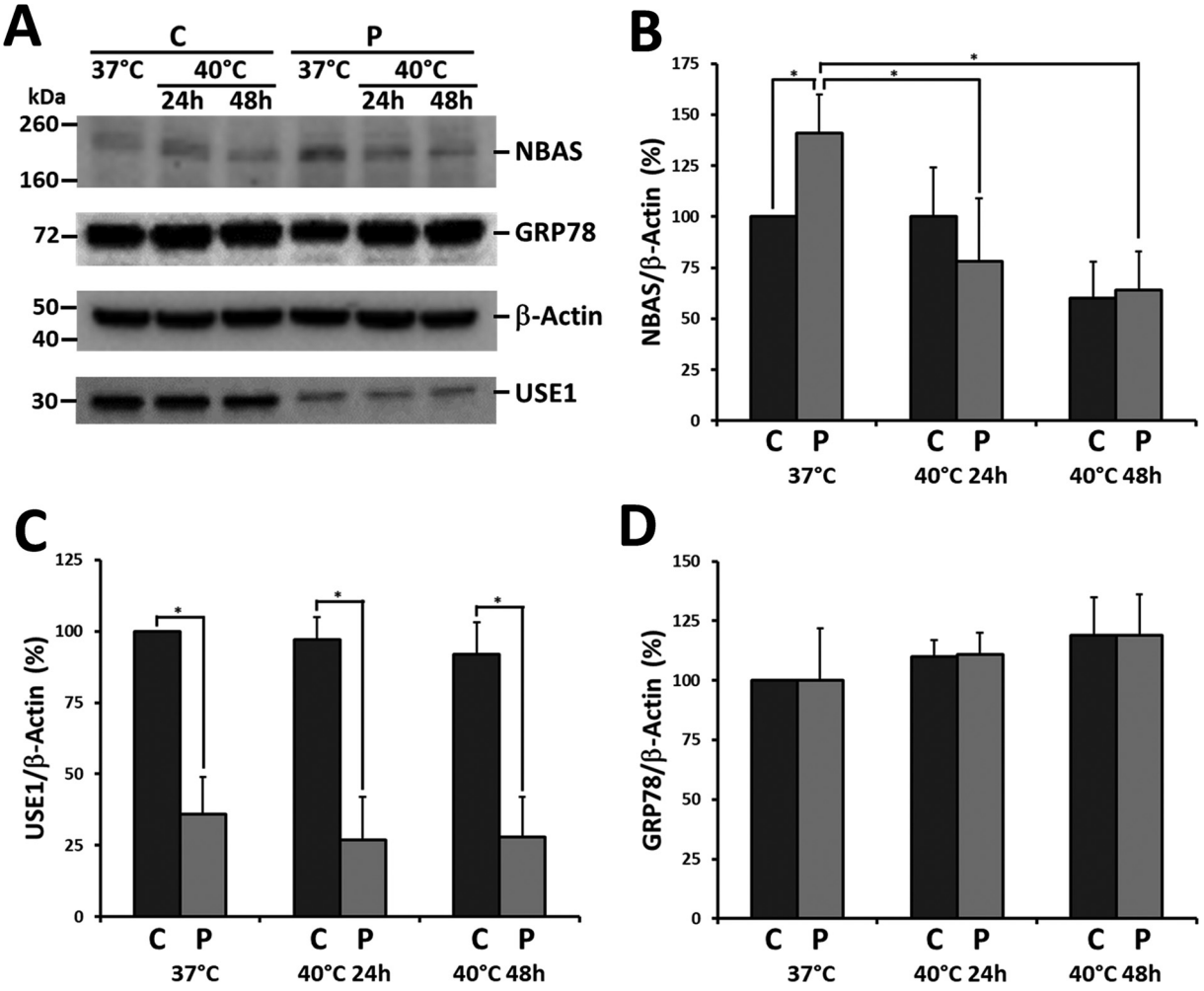

Fig. 4. Thermal stability of NBAS protein analysis and ER stress. (A) Western blot analysis. The patient (P) and the control (C) fibroblast cell line were cultivated at 37 °C and then heated to 40 °C (during 24 or 48 h). The panel shows a representative immunoblotting of NBAS, USE1, GRP78 and β-actin. Densitometry analysis of the peak density normalized over β-actin of NBAS (B), USE1 (C) and GRP78 (D). Data were the mean (±SD) of three independent experiments, and protein amount in the control at 37 °C was set as 100%. $^{*}P < 0.05$.

(Fig. 5B, merge) showed that COL1A2 retention in cells overexpressing the mutated protein was significantly higher than in the remaining cells (Fig. 5E). Finally, COL1A2 is retained into the cell, probably in ER (Fig. 5B, merge2).

4. Discussion

Herein, we describe a patient with infantile fever-dependent RALF and OI (Fig. 1). Using WES, we were able to identify two compound heterozygous variants in *NBAS* (NBAS: p.[(Leu422Pro)];[(Arg517Cys)]) and one heterozygous variant in *P4HB* (PDI: p.[(Lys65Arg)]) (Table 1).

NBAS is involved in retrograde vesicular transport at the ER, and interacts directly with the t-SNARE USE1 together with ZW10, and v-SNARE SEC22b, forming the syntaxin 18 complex [1,2]. In addition, it acts as a mediator of the NMD modulating, among others, genes involved in bone development [3], and in the formation of large transport vesicle at the ER exit site in the secretory pathway [5]. Variants in *NBAS* have been associated with ILFS2 and SOPH syndrome. The homozygous variant c.5741G > A (p.Arg1914His) in *NBAS* that resulted in SOPH syndrome was described in 2010 in 33 patients, and some of these patients showed abnormalities in bone, from delayed bone age to osteoporosis [6]. In 2015, other variants in *NBAS* were reported in 11 patients from 10 families with fever-dependent RALF starting in infancy that later was renamed as ILFS2 [2]. After that, numerous cases of patients with NBAS deficiency have been reported. Currently, 126 patients from 112 families with 101 variants in *NBAS* have been published or reported at conferences [7–10]. Thus, there are patients with SOPH syndrome without liver failure [6,7,10,22], with ILFS2 without SOPH syndrome [2,7,8,21,23], and combined phenotypes [2,7–9,21], including patients with severe skeletal system involvement [2,7,8,21,24,25] and OI [7,9,11]. Then, the phenotype most frequent in patients with *NBAS* variants is fever-dependent RALF or ILFS2. In these patients, the levels of NBAS protein in fibroblasts were lower than in controls (up to 75%), and concomitant with this reduction, the levels of the USE1 were also decreased [2,11,21]. These levels must be sufficient for its normal function (including in liver) under afebrile conditions. However, the mutated NBAS protein levels in fibroblasts suffer a further decrease when the temperature increase from 37 to 40 °C (equivalent to febrile conditions), indicating a variant-dependent thermal instability [21]. In a unique case, the mutated NBAS protein levels were not significantly changed, but the levels of USE1 were reduced significantly at 37 and 40 °C [23]. Therefore, the hypothesized cause of ILFS2 is the reduced mutated NBAS protein levels together with its thermal instability, and/or the loss of NBAS-USE1 interaction that causes an alteration of Golgi-to-ER retrograde vesicular trafficking. This alteration could induce ER stress and liver cell apoptosis under febrile conditions, which would lead to acute liver failure [2,21,23,26]. However, our patient has a higher level of NBAS protein compared to controls (Fig. 3A, B) although his mRNA expression is lower than in controls (Fig. 3C). It was not possible to determine if both alleles were involved in the overexpression of the

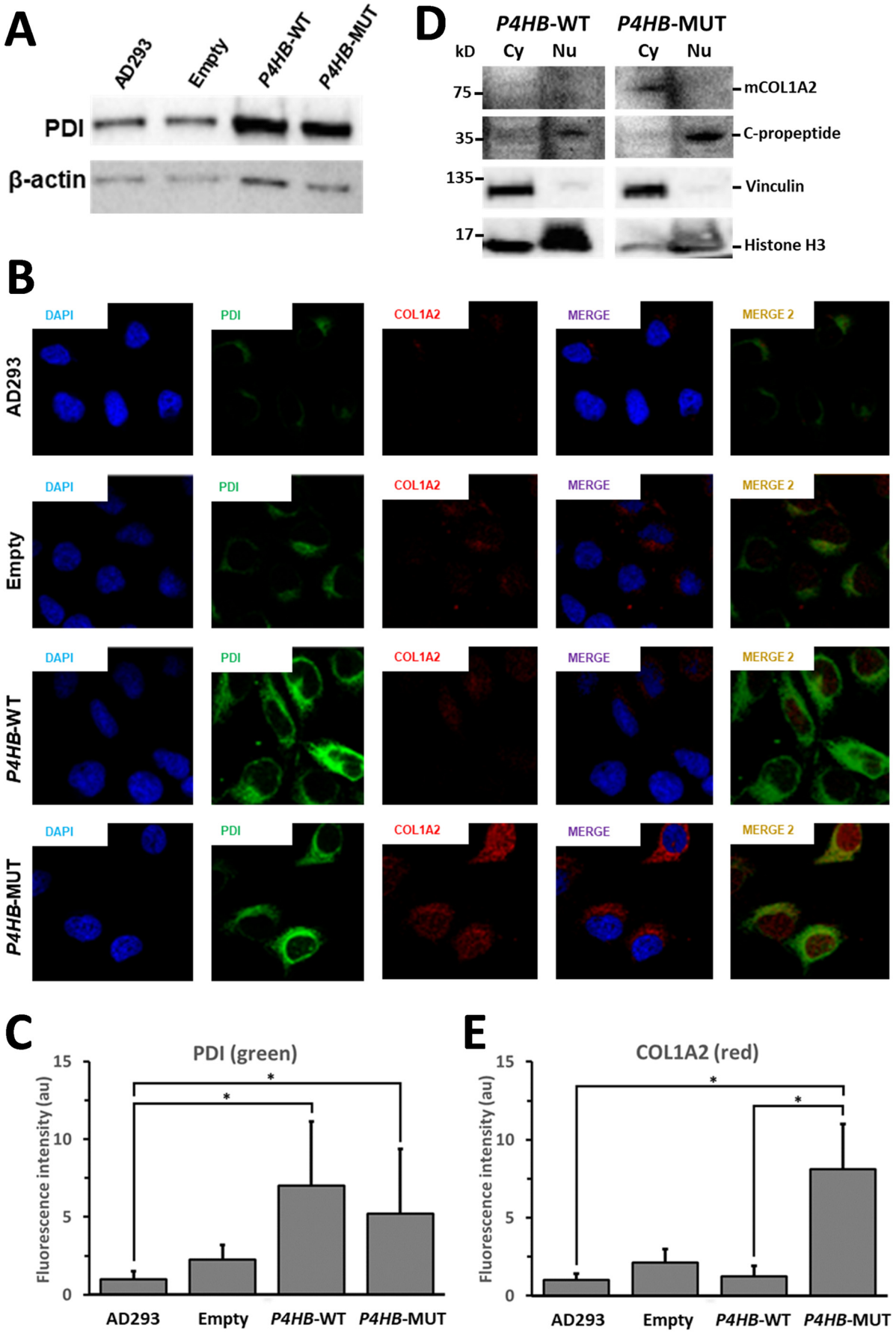
A
AD293
Empty
P4HB-WT
P4HB-MUT
PDI
β-actin
D
P4HB-WT
P4HB-MUT
kD
Cy
Nu
Cy
Nu
75
35
135
17
mCOL1A2
C-propeptide
Vinculin
Histone H3
B
DAPI
PDI
COL1A2
MERGE
MERGE 2
AD293
Empty
P4HB-WT
P4HB-MUT
C
PDI (green)
Fluorescence intensity (au)
15
10
5
0
*
*
AD293
Empty
P4HB-WT
P4HB-MUT
E
COL1A2 (red)
Fluorescence intensity (au)
15
10
5
0
*
*
AD293
Empty
P4HB-WT
P4HB-MUT

protein. This could be due to a compensatory response at translational level to a less functional protein or to a higher protein stability [2]. The levels of NBAS in our patient suffer also a great decrease when the temperature increase from 37 to 40 °C (Fig. 4A, B), demonstrating that these variants also produce thermal instability. Furthermore, the patient showed a large decrease on the levels of USE1 even at 37 °C (Fig. 4A, C). Despite NBAS overexpression, as the two variants are located in the interaction domain with USE1, they may impair NBAS-USE1 binding resulting in a loss of protein stability of USE1 [2,21,23]. The loss of this interaction may alter the correct functioning of Golgi-to-ER retrograde vesicle trafficking, which leads to diseases including liver dysfunction [27]. Therefore, the variants in *NBAS* are responsible of the liver phenotype. On the other hand, no evidence for increased ER stress was found in our patient, since the levels of the ER stress marker GRP78 were similar to the control (Fig. 4A, D) [28]. These data could argue against the role of ER stress in the pathomechanism of the liver phenotype, unlike that previously proposed by Haack et al. [2]. However, it cannot be ruled out that ER stress may play a role in hepatocytes, or through a pathway other than the induction of GRP78 [29].

OI is a heterogeneous group of disorders that causes bone fragility and deformity. It is mostly caused by variants in *COL1A1* or *COL1A2*, the genes encoding collagen type I alpha chains. However, other genes involved in the post-translational modification of collagen type I or in the regulation of bone homeostasis have been reported as causative of rare forms of OI [30]. The collagen type I was retained into the cell, probably in the ER within the patient's fibroblasts (Fig. 3A, α-COL1A2), and this could be the mechanism of the OI [31,32].

In addition to its role in retrograde vesicular transport, NBAS was also shown to modulate genes involved in bone development as a mediator of the ER-NMD [3,4]. In the patient, the NMD pathway dependent of NBAS was altered as demonstrated by the downregulation of two of its targets, *MGP* and *SMG5* (Fig. 3C). Furthermore, the decrease of MGP activity, which regulates osteoclast differentiation and bone resorption, would be compatible with the described bone phenotype (OI) [33].

Moreover, it has been shown that depletion of NBAS in fibroblasts inhibits collagen VII secretion and arrests collagen in the ER, indicating an additional role in the formation of large transport vesicle at the ER exit site in the secretory pathway [5]. Thus, the bone phenotype in NBAS patients, such as skeletal dysplasia and Pelger-Huët anomaly in SOPH syndrome, and the osteoporosis and OI shown in some patients could be explained by the reduction of collagen secretion [9]. Our patient belongs to the β-propeller clinical subgroup of NBAS-associated disease because he has a combined severe phenotype (ILFS2 and OI) and one variant is situated in the β-propeller domain (p.Leu422Pro) and the other (p.Arg517Cys) between β-propeller and Sec39 domain [7]. The protein change p.Arg517Cys has been reported in three additional patients, and interestingly, one patient showed an important bone involvement including pathologic fractures, while the other two patients did not [7]. The other variant is new and has not been previously reported in any patient. Therefore, the variants in *NBAS* could be also responsible of the bone phenotype.

However, the patient has a heterozygous variant in *P4HB*, and variants in this gene have been associated with CLCRP1, an OI-like disorder. The CLCRP1 was first described phenotypically in 1987 in two unrelated patients with bone fragility with multiple fractures, deformities of bone, craniosynostosis, ocular proptosis, hydrocephalus, facial dysmorphism, and normal intelligence [14]. Later, in 2015 these patients were genetically diagnosed harboring the same heterozygous missense variant in *P4HB* (p.Tyr393Cys) [15]. In one patient, the variant was *de novo*, whereas in the other the variant was transmitted from the clinically unaffected father who was mosaic carrier of the variant. After that, only other 6 patients have been described: two with the same *de novo* variant [16,17], one with a new *de novo* variant (p.Cys400Arg) [18], other with a *de novo* deletion of exon 5 to 8 [19], and finally two patients (father and daughter) with other missense variant (p.His231Pro) [20]. Two of these missense variants (p.Tyr393Cys and p.Cys400Arg) are located in the Thioredoxin 2 domain, affecting the catalytic active site –CXXC– (Fig. 2H), while the other (p.His231Pro) is in the non-catalytic domain involved in substrate recognition [13,34]. The heterozygous variant in *P4HB* of our patient is located close to the catalytic active site of the Thioredoxin 1 domain (Fig. 2H), and similar to the patient 1 described in 2015 [15], the variant was transmitted from the clinically unaffected mother who was mosaic carrier.

It has been shown that PDI interacts with proteins during their folding and assembly pathways in the ER, functioning as a quality control, whereby unassembled proteins are retained in the ER [12] and the correctly folded proteins are released [35]. PDI is a key enzyme for post-translational modifications of collagen type I at three levels: hydroxylation of prolines (PDI is part of P4H, the protein that hydroxylates many proline residues on the procollagen type I alpha chains), procollagen assembly (PDI catalyzes the formation of disulfide bonds), and quality control (acting as molecular chaperone during the assembly of procollagen type I and preventing its premature assembly or aggregation) [35]. In order to study the role of PDI variant in the bone phenotype, the wild-type and mutated version of PDI were overexpressed in the AD293 cell line (Fig. 5A) and the retention of collagen in the cells was evaluated. The overexpression of the mutated PDI protein in AD293 cells (Fig. 5) caused a greater retention of the collagen in the cells (Fig. 5B, E), demonstrating that the variant in PDI is the cause of collagen retention in the cells. However, in patients described so far, the collagen type I protein analyses in skin fibroblasts were reported normal [15,16]. Notwithstanding the above, our data suggest that the secretion of collagen type I could be the most probably cause of the OI in our patient [31,32]. On the other hand, the mosaicism of *P4HB* variant in the mother, without bone symptoms, could be explained due to the variant not being present or being present in a very low proportion in the skeletal system. But it could also happen that the variant acts as a genetic modifier of the bone phenotype that the two variants in *NBAS* would produce in the patient.

At this point, we can state that the variant in *P4HB* is involved in the OI, as well as that *NBAS* variants are probably also involved in the patient's bone phenotype. For this reason, we cannot clarify if the variant in *P4HB* is acting as a genetic modifier for *NBAS* variants, or if it is indeed responsible for an OI dominant phenotype.

In conclusion, this is the first report of a patient with ILFS2 and OI due to variants in two different genes, *NBAS* and *P4HB*. The two variants in *NBAS* are responsible for liver phenotype (ILFS2), and the variant in *P4HB* is involved in the bone phenotype (OI).

Declaration of Competing Interest

The authors declare no conflict of interest.

Fig. 5. Functional study of PDI. (A) Molecular analysis of PDI overexpression. AD293 cells were transfected with the plasmid pREP4 empty or containing the ORF of wild-type (*P4HB*-WT) or mutated (*P4HB*-MUT) PDI. Cell lysate from these cells were analyzed by SDS-PAGE and western blotting using the antibodies against PDI and β-actin. (B) Representative immunofluorescent images of collagen retention in AD293 cells overexpressing wild-type (*P4HB*-WT) or mutated (*P4HB*-MUT) PDI. Columns are: left DAPI (nuclei; blue), PDI (green), COL1A2 (red), merge DAPI/COL1A2, and merge2 PDI/COL1A2 images. (D) Subcellular fractionation of AD293 cells overexpressing wild-type or mutated PDI. Vinculin was used as cytoplasmic (Cy) marker protein and Histone H3 as a marker of the nucleus (Nu). Quantification of the vesicular pattern of PDI (green fluorescence) (C) and cytoplasmic COL1A2 (red fluorescence in merge) (E). Total fluorescence was normalized to the control (AD293). Data were the mean (±SD) of three independent experiments. $^{*}P < 0.05$.

Acknowledgements

The authors thank the patient and his family for their contribution. This work was supported by the Spanish Instituto de Salud Carlos III (ISCIII) and European Regional Development Fund (ERDF) (grant PI17/00487 to F.M-A.). F.J.C-V. was supported by fellowship from the Instituto de Investigación Hospital 12 de Octubre (i+12). M.E.R-G. was supported by fellowship from ISCIII and ERDF (PI17/00487).

References

[1] T. Aoki, S. Ichimura, A. Itoh, M. Kuramoto, T. Shinkawa, T. Isobe, M. Tagaya, Identification of the neuroblastoma-amplified gene product as a component of the syntaxin 18 complex implicated in Golgi-to-endoplasmic reticulum retrograde transport, Mol. Biol. Cell 20 (2009) 2639–2649, https://doi.org/10.1091/mbc.E08-11-1104.

[2] T.B. Haack, C. Staufner, M.G. Kopke, B.K. Straub, S. Kolker, C. Thiel, P. Freisinger, I. Baric, P.J. McKiernan, N. Dikow, I. Harting, F. Beisse, P. Burgard, U. Kotzaeridou, J. Kuhr, U. Himbert, R.W. Taylor, F. Distelmaier, J. Vockley, L. Ghaloul-Gonzalez, J. Zschocke, L.S. Kremer, E. Graf, T. Schwarzmayr, D.M. Bader, J. Gagneur, T. Wieland, C. Terrile, T.M. Strom, T. Meitinger, G.F. Hoffmann, H. Prokisch, Biallelic Mutations in NBAS Cause Recurrent Acute Liver Failure with Onset in Infancy, Am. J. Hum. Genet. 97 (2015) 163–169, https://doi.org/10.1016/j.ajhg.2015.05.009.

[3] D. Longman, N. Hug, M. Keith, C. Anastasaki, E.E. Patton, G. Grimes, J.F. Caceres, DHX34 and NBAS form part of an autoregulatory NMD circuit that regulates endogenous RNA targets in human cells, zebrafish and Caenorhabditis elegans, Nucleic Acids Res. 41 (2013) 8319–8331, https://doi.org/10.1093/nar/gkt585.

[4] D. Longman, K.A. Jackson-Jones, M.M. Maslon, L.C. Murphy, R.S. Young, J.J. Stoddart, N. Hug, M.S. Taylor, D.K. Papadopoulos, J.F. Caceres, Identification of a localized nonsense-mediated decay pathway at the endoplasmic reticulum, Genes Dev. 34 (2020) 1075–1088, https://doi.org/10.1101/gad.338061.120.

[5] I. Raote, M. Ortega-Bellido, A.J. Santos, O. Foresti, C. Zhang, M.F. Garcia-Parajo, F. Campelo, V. Malhotra, TANGO1 builds a machine for collagen export by recruiting and spatially organizing COPII, tethers and membranes, Elife 7 (2018) https://doi.org/10.7554/eLife.32723.

[6] N. Maksimova, K. Hara, I. Nikolaeva, T. Chun-Feng, T. Usui, M. Takagi, Y. Nishihira, A. Miyashita, H. Fujiwara, T. Oyama, A. Nogovicina, A. Sukhomyasova, S. Potapova, R. Kuwano, H. Takahashi, M. Nishizawa, O. Onodera, Neuroblastoma amplified sequence gene is associated with a novel short stature syndrome characterised by optic nerve atrophy and Pelger-Huet anomaly, J. Med. Genet. 47 (2010) 538–548, https://doi.org/10.1136/jmg.2009.074815.

[7] C. Staufner, B. Peters, M. Wagner, S. Alameer, I. Baric, P. Broue, D. Bulut, J.A. Church, E. Crushell, B. Dalgic, A.M. Das, A. Dick, N. Dikow, C. Dionisi-Vici, F. Distelmaier, N.E. Bozbulut, F. Feillet, E. Gonzales, N. Hadzic, F. Hauck, R. Hegarty, M. Hempel, T. Herget, C. Klein, V. Konstantopoulou, R. Kopajtich, A. Kuster, M.W. Laass, E. Lainka, C. Larson-Nath, A. Leibner, E. Lurz, J.A. Mayr, P. McKiernan, K. Mention, U. Moog, N.O. Mungan, K.M. Riedhammer, R. Santer, I.V. Palafoll, J. Vockley, D.S. Westphal, A. Wiedemann, S.B. Wortmann, G.D. Diwan, R.B. Russell, H. Prokisch, S.F. Garbade, S. Kolker, G.F. Hoffmann, D. Lenz, Defining clinical subgroups and genotype-phenotype correlations in NBAS-associated disease across 110 patients, Genet. Med. 22 (2020) 610–621, https://doi.org/10.1038/s41436-019-0698-4.

[8] Z.D. Li, K. Abuduxikuer, J. Zhang, Y. Yang, Y.L. Qiu, Y. Huang, X.B. Xie, Y. Lu, J.S. Wang, NBAS disease: 14 new patients, a recurrent mutation, and genotype-phenotype correlation among 24 Chinese patients, Hepatol. Res. 50 (2020) 1306–1315, https://doi.org/10.1111/hepr.13559.

[9] M. Ritelli, E. Palagano, V. Cinquina, F. Beccagutti, N. Chiarelli, D. Strina, I.F. Hall, A. Villa, C. Sobacchi, M. Colombi, Genome-first approach for the characterization of a complex phenotype with combined NBAS and CUL4B deficiency, Bone 140 (2020), 115571. https://doi.org/10.1016/j.bone.2020.115571.

[10] Y. Lacassie, B. Johnson, G. Lay-Son, R. Quintana, A. King, F. Cortes, C. Alvarez, R. Gomez, A. Vargas, S. Chalew, A. King, S. Guardia, R.U. Sorensen, S. Aradhya, Severe SOPH syndrome due to a novel NBAS mutation in a 27-year-old woman-review of this pleiotropic, autosomal recessive disorder: mystery solved after two decades, Am. J. Med. Genet. A 182 (2020) 1767–1775, https://doi.org/10.1002/ajmg.a.61597.

[11] M. Balasubramanian, J. Hurst, S. Brown, N.J. Bishop, P. Arundel, C. DeVile, R.C. Pollitt, L. Crooks, D. Longman, J.F. Caceres, F. Shackley, S. Connolly, J.H. Payne, A.C. Offiah, D. Hughes, D.D.D. Study, M.J. Parker, W. Hide, T.M. Skerry, Compound heterozygous variants in NBAS as a cause of atypical osteogenesis imperfecta, Bone 94 (2017) 65–74, https://doi.org/10.1016/j.bone.2016.10.023.

[12] M.J. Bottomley, M.R. Batten, R.A. Lumb, N.J. Bulleid, Quality control in the endoplasmic reticulum: PDI mediates the ER retention of unassembled procollagen C-propeptides, Curr. Biol. 11 (2001) 1114–1118, https://doi.org/10.1016/s0960-9822(01)00317-7.

[13] H. Ali Khan, B. Mutus, Protein disulfide isomerase a multifunctional protein with multiple physiological roles, Front. Chem. 2 (2014) 70, https://doi.org/10.3389/fchem.2014.00070.

[14] D.E. Cole, T.O. Carpenter, Bone fragility, craniosynostosis, ocular proptosis, hydrocephalus, and distinctive facial features: a newly recognized type of osteogenesis imperfecta, J. Pediatr. 110 (1987) 76–80, https://doi.org/10.1016/s0022-3476(87)80292-5.

[15] F. Rauch, S. Fahiminiya, J. Majewski, J. Carrot-Zhang, S. Boudko, F. Glorieux, J.S. Mort, H.P. Bachinger, P. Moffatt, Cole-Carpenter syndrome is caused by a heterozygous missense mutation in P4HB, Am. J. Hum. Genet. 96 (2015) 425–431, https://doi.org/10.1016/j.ajhg.2014.12.027.

[16] M. Balasubramanian, R. Padidela, R.C. Pollitt, N.J. Bishop, M.Z. Mughal, A.C. Offiah, B.E. Wagner, J. McCaughey, D.J. Stephens, P4HB recurrent missense mutation causing Cole-Carpenter syndrome, J. Med. Genet. 55 (2018) 158–165, https://doi.org/10.1136/jmedgenet-2017-104899.

[17] T. Porntaveetus, T. Theerapanon, C. Srichomthong, V. Shotelersuk, Cole-Carpenter syndrome in a patient from Thailand, Am. J. Med. Genet. A 176 (2018) 1706–1710, https://doi.org/10.1002/ajmg.a.40358.

[18] Y.J. Cao, H. Zhang, Z.L. Zhang, Novel mutations in the Wnt1, Tmem38b, P4hb, and Pls3 genes in four unrelated Chinese families with osteogenesis imperfecta, Endocr. Pract. 25 (2019) 230–241, https://doi.org/10.4158/EP-2018-0443.

[19] L. Ouyang, F. Yang, Cole-Carpenter syndrome-1 with a de novo heterozygous deletion in the P4HB gene in a Chinese girl: a case report, Medicine (Baltimore) 96 (2017), e9504. https://doi.org/10.1097/MD.0000000000009504.

[20] L. Li, D. Zhao, W. Zheng, O. Wang, Y. Jiang, W. Xia, X. Xing, M. Li, A novel missense mutation in P4HB causes mild osteogenesis imperfecta, Biosci. Rep. 39 (2019) https://doi.org/10.1042/BSR20182118.

[21] C. Staufner, T.B. Haack, M.G. Kopke, B.K. Straub, S. Kolker, C. Thiel, P. Freisinger, I. Baric, P.J. McKiernan, N. Dikow, I. Harting, F. Beisse, P. Burgard, U. Kotzaeridou, D. Lenz, J. Kuhr, U. Himbert, R.W. Taylor, F. Distelmaier, J. Vockley, L. Ghaloul-Gonzalez, J.A. Ozolek, J. Zschocke, A. Kuster, A. Dick, A.M. Das, T. Wieland, C. Terrile, T.M. Strom, T. Meitinger, H. Prokisch, G.F. Hoffmann, Recurrent acute liver failure due to NBAS deficiency: phenotypic spectrum, disease mechanisms, and therapeutic concepts, J. Inherit. Metab. Dis. 39 (2016) 3–16, https://doi.org/10.1007/s10545-015-9896-7.

[22] X. Li, Q. Cheng, N. Li, G. Chang, Y. Ding, J. Li, Y. Shen, J. Wang, X. Wang, SOPH syndrome with growth hormone deficiency, normal bone age, and novel compound heterozygous mutations in NBAS, Fetal Pediatr. Pathol. 37 (2018) 404–410, https://doi.org/10.1080/15513815.2018.1509406.

[23] S. Ono, J. Matsuda, E. Watanabe, H. Akaike, H. Teranishi, I. Miyata, T. Otomo, Y. Sadahira, T. Mizuochi, H. Kusano, M. Kage, H. Ueno, K. Yoshida, Y. Shiraishi, K. Chiba, H. Tanaka, S. Miyano, S. Ogawa, Y. Hayashi, H. Kanegane, K. Ouchi, Novel neuroblastoma amplified sequence (NBAS) mutations in a Japanese boy with fever-triggered recurrent acute liver failure, Hum. Genome. Var. 6 (2019) 2, https://doi.org/10.1038/s41439-018-0035-5.

[24] J.M. Capo-Chichi, C. Mehawej, V. Delague, C. Caillaud, I. Khneisser, F.F. Hamdan, J.L. Michaud, Z. Kibar, A. Megarbane, Neuroblastoma amplified sequence (NBAS) mutation in recurrent acute liver failure: confirmatory report in a sibship with very early onset, osteoporosis and developmental delay, Eur. J. Med. Genet. 58 (2015) 637–641, https://doi.org/10.1016/j.ejmg.2015.11.005.

[25] Y. Sunwoo, Y.M. Kim, E.N. Kim, S.H. Oh, B.H. Lee, Severe form of neuroblastoma amplified sequence deficiency in an infant with recurrent acute liver failure, Pediatr. Int. 60 (2018) 302–304, https://doi.org/10.1111/ped.13476.

[26] H. Malhi, R.J. Kaufman, Endoplasmic reticulum stress in liver disease, J. Hepatol. 54 (2011) 795–809, https://doi.org/10.1016/j.jhep.2010.11.005.

[27] A. Frappaolo, A. Karimpour-Ghahnavieh, S. Sechi, M.G. Giansanti, The close relationship between the golgi trafficking machinery and protein glycosylation, Cells 9 (2020) https://doi.org/10.3390/cells9122652.

[28] M. Hammadi, A. Oulidi, F. Gackiere, M. Katsogiannou, C. Slomianny, M. Roudbaraki, E. Dewailly, P. Delcourt, G. Lepage, S. Lotteau, S. Ducreux, N. Prevarskaya, F. Van Coppenolle, Modulation of ER stress and apoptosis by endoplasmic reticulum calcium leak via translocon during unfolded protein response: involvement of GRP78, FASEB J. 27 (2013) 1600–1609, https://doi.org/10.1096/fj.12-218875.

[29] F. Cabral Miranda, J. Adao-Novaes, W.W. Hauswirth, R. Linden, H. Petrs-Silva, L.B. Chiarini, CHIP, a carboxy terminus HSP-70 interacting protein, prevents cell death induced by endoplasmic reticulum stress in the central nervous system, Front. Cell. Neurosci. 8 (2014) 438, https://doi.org/10.3389/fncel.2014.00438.

[30] A. El-Gazzar, W. Hogler, Mechanisms of Bone Fragility: From Osteogenesis Imperfecta to Secondary Osteoporosis, Int J Mol Sci 22, 2021https://doi.org/10.3390/ijms22020625.

[31] E. Makareeva, G. Sun, L.S. Mirigian, E.L. Mertz, J.C. Vera, N.A. Espinoza, K. Yang, D. Chen, T.E. Klein, P.H. Byers, S. Leikin, Substitutions for arginine at position 780 in triple helical domain of the alpha1(I) chain alter folding of the type I procollagen molecule and cause osteogenesis imperfecta, PLoS One 13 (2018), e0200264. https://doi.org/10.1371/journal.pone.0200264.

[32] U. Lindert, M. Gnoli, M. Maioli, M.F. Bedeschi, L. Sangiorgi, M. Rohrbach, C. Giunta, Insight into the pathology of a COL1A1 signal peptide heterozygous mutation leading to severe osteogenesis imperfecta, Calcif. Tissue Int. 102 (2018) 373–379, https://doi.org/10.1007/s00223-017-0359-z.

[33] Y. Zhang, L. Zhao, N. Wang, J. Li, F. He, X. Li, S. Wu, Unexpected role of matrix gla protein in osteoclasts: inhibiting osteoclast differentiation and bone resorption, Mol. Cell. Biol. 39 (2019) https://doi.org/10.1128/MCB.00012-19.

[34] G. Kozlov, P. Maattanen, D.Y. Thomas, K. Gehring, A structural overview of the PDI family of proteins, FEBS J. 277 (2010) 3924–3936, https://doi.org/10.1111/j.1742-4658.2010.07793.x.

[35] R. Wilson, J.F. Lees, N.J. Bulleid, Protein disulfide isomerase acts as a molecular chaperone during the assembly of procollagen, J. Biol. Chem. 273 (1998) 9637–9643, https://doi.org/10.1074/jbc.273.16.9637.